

# Ultrafast 2D IR Vibrational Echo Spectroscopy

JUNRONG ZHENG, KYUNGWON KWAK, AND  
M. D. FAYER\*

Department of Chemistry, Stanford University,  
Stanford, California 94305

Received May 10, 2006

## ABSTRACT

The experimental technique and applications of ultrafast two-dimensional infrared (2D IR) vibrational echo spectroscopy are presented. Using ultrashort infrared pulses and optical heterodyne detection to provide phase information, unique information can be obtained about the dynamics, interactions, and structures of molecular systems. The form and time evolution of the 2D IR spectrum permits examination of processes that cannot be studied with linear infrared absorption experiments. Three examples are given: organic solute–solvent complex chemical exchange, dynamics of the hydrogen-bond network of water, and assigning peaks in an IR spectrum of a mixture of species.

## I. Introduction

Ultrafast 2D IR vibrational echo spectroscopy<sup>1–11</sup> is an ultrafast IR analog of 2D NMR<sup>12</sup> that directly probes the structural degrees of freedom of molecules.<sup>13</sup> The 2D IR vibrational echo technique involves a three-pulse sequence that induces and then probes the coherent evolution of excitations (vibrations) of a molecular system. The first pulse in the sequence causes vibrational modes of a molecular ensemble to initially “oscillate” with the identical phase. The later pulses generate observable signals that are sensitive to changes in environments of individual molecules during the experiment, even if the aggregate populations in distinct environments do not change. For example, formation and dissociation of molecular complexes under thermal equilibrium conditions can be observed. The 2D IR vibrational echo spectrum can also display intramolecular interactions and dynamics that are

Junrong Zheng was born in Chaozhou, China, in 1973. He obtained a B.S. degree (1997) in Chemistry and M.S. degree in Polymer Chemistry (2000) from Beijing University and another M.S. degree in Polymer Physics (2003) from Rensselaer Polytechnic Institute. Currently he is a doctoral candidate in physical chemistry at Stanford University in the group of Professor Michael D. Fayer. His research concentrates on development and applications of 2D IR vibrational echo spectroscopy.

Kyungwon Kwak was born in Ansong, Korea, in 1973. He received his B.A. degree in Chemistry from Korea University in 1999 and earned his M.S. degree in Physical Chemistry from Korea University with Professor Minhaeng Cho in 2001. Currently he is a doctoral candidate in physical chemistry at Stanford University in the group of Professor Michael D. Fayer. His research concentrates on development and applications of 2D IR vibrational echo spectroscopy.

Michael D. Fayer was born in Los Angeles, CA, in 1947. He obtained a B.S. (1969) and Ph.D. (1974) degrees in Chemistry from the University of California at Berkeley. He joined the faculty at Stanford University in 1974 and is now the David Mulvane Ehrsam and Edward Curtis Franklin Professor of Chemistry. His research interests include dynamics and intermolecular interactions in condensed-matter systems and biological molecules investigated with ultrafast nonlinear visible and infrared optical methods and theory.

not observable in linear vibrational absorption experiments. A critical difference between the 2D IR and NMR variants is that the IR pulse sequence is sensitive to dynamics on timescales 6–10 orders of magnitude faster than the NMR pulse sequence.

2D IR vibrational echo spectroscopy has several characteristics that make it a useful tool for the study of problems involving rapid dynamics under thermal equilibrium in condensed phases, e.g., fast chemical exchange reactions, solute/solvent interactions, water dynamics, and intramolecular interactions. Such problems are important and ubiquitous in nature and difficult to study by other means. 2D IR vibrational echo experiments have temporal resolution < 50 fs, which is sufficiently fast to study the fastest chemical processes. In contrast to electronic excitation, the vibration excitation associated with 2D IR experiments produces a negligible perturbation of a molecular system that does not change the chemical properties of the samples. 2D IR experiments can also be useful as a tool for chemical structural analysis by revealing the relationship among different mechanical degrees of freedom of a molecular<sup>14,15</sup> or biomolecular system.<sup>3,10,16</sup> 2D IR vibrational echo experiments have been successfully applied to study fast chemical exchange reactions and solution dynamics,<sup>9,17,18</sup> water dynamics,<sup>19,20</sup> hydrogen network evolution,<sup>6</sup> intramolecular vibrational energy relaxations,<sup>5</sup> protein structures and dynamics,<sup>3,10,16,21</sup> and mixed chemicals analysis.<sup>15</sup>

In 1995 an *Accounts of Chemical Research* article was published<sup>22</sup> summarizing recent fast condensed phase vibrational echo experiments.<sup>1,23,24</sup> The experiments were 1D with a time resolution of ~1 ps. Since those first experiments, the field has advanced greatly. Vibrational echoes have gone multidimensional with full phase information, significantly increasing the types of information that can be obtained. Furthermore, tabletop laser systems now provide sub 50 fs IR pulses, making 2D IR vibrational echo spectroscopy increasingly available to a wide range of researchers. In this Account we will first introduce the experimental technique and then describe its applications in the study of chemical exchange reactions,<sup>9,18</sup> water dynamics,<sup>19</sup> and chemical analysis.<sup>15</sup> Interesting topics that are not covered here are experiments by Tokmakoff and co-workers on the coupling between vibrational modes,<sup>14</sup> population relaxation,<sup>5</sup> and structure and dynamics of proteins,<sup>10</sup> experiments by Hochstrasser and co-workers on solution dynamics of small molecules,<sup>25</sup> hydrogen-bond chemical exchange,<sup>17</sup> and small peptide models of biological systems,<sup>26</sup> experiments by Zanni and co-workers on fifth-order vibrational echo spectroscopy<sup>8</sup> and membrane peptides,<sup>7</sup> and experiments by Fayer and co-workers on hydrogen-bonded oligomers,<sup>6</sup> nanoscopic water,<sup>27</sup> and protein structure and dynamics.<sup>16,28</sup>

## II. Experimental Method

In a 2D IR vibrational echo experiment three ultrashort IR pulses tuned to the frequency of the vibrational modes

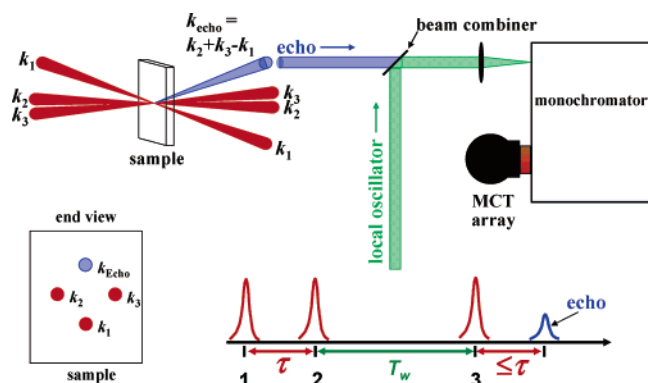


**FIGURE 1.** Schematic of the ultrafast 2D vibrational echo spectrometer showing the wave vectors ( $k_i$ ) and the vibrational echo pulse sequence.

of interest are crossed in the sample. Because the pulses are very short, they have a broad bandwidth, which makes it possible to simultaneously excite a number of vibrational modes or a very broad spectral feature such as the hydroxyl stretch band of water. The times between pulses 1 and 2 and pulses 2 and 3 are called  $\tau$  and  $T_w$ , respectively (see Figure 1; a time period refers to the time between the pulse peaks). At a time  $\leq \tau$  after the third pulse, a fourth IR pulse is emitted in a unique direction. This is the vibrational echo, the signal in the experiments. The vibrational echo is the infrared vibrational equivalent of the magnetic resonance spin echo<sup>29</sup> and the electronic excitation photon echo.<sup>30</sup> Before going into more quantitative detail, a qualitative description is given of how the vibrational echo pulse arises and how it is possible to obtain phase information, not just the intensity, from the vibrational echo.

The first pulse in the sequence places the vibrational oscillators into a coherent superposition state of the vibrational ground state (0) and vibrational first excited state (1) with all of the oscillators initially oscillating in phase. The initial macroscopic phase relationships among the oscillators decay rapidly. This is called free induction decay. The phase relationships can decay for a number of reasons. Several peaks in the IR spectrum may be excited. These are at different frequencies, so the vibrational oscillators oscillate at different intrinsic frequency. Even for a single mode, molecules in different environments, e.g., different local solvent structures, will have different oscillator frequencies, which is called inhomogeneous broadening. In addition, there are dynamic interactions with the environment, e.g., local solvent structure fluctuations, which cause the frequency of a given oscillator to evolve in time. These frequency fluctuations are called dynamic dephasing and spectral diffusion. The rest of the pulse sequence can preserve information about the phase relationships that are seemingly lost during the free induction decay. Only the spectral diffusion at sufficiently long time can totally destroy the phase relations among the oscillators that cannot be recovered by the rest of the pulse sequence. However, even then, the signal is not zero because the initial two pulses also set up a spatial relationship among the oscillators that contributes to the signal.

The second pulse in the sequence stores the phase (and spatial) information induced by the first pulse as a complex frequency and spatial pattern of differences of the populations of the 0 and 1 vibrational states. After the waiting period,  $T_w$ , the third pulse again generates coherent superposition states of the oscillators. Initially the oscillators are not in phase, but the pulse sequence initiates a rephasing process.<sup>29</sup> At a time  $\leq \tau$  after the third pulse, the vibrational oscillators are again oscillating in phase. Each vibrational oscillator has associated with it a microscopic oscillating electric dipole. When rephasing has occurred and all of the oscillators are in phase, the sample has a macroscopic oscillating electric dipole. A macroscopic oscillating electric dipole emits radiation, which is the source of the vibrational echo. The vibrational echo pulse is short because the oscillators again get out of phase just as they did after the first pulse.

Both the intensity of the 2D vibrational echo pulse and its time structure contain important information. If the echo pulse is sent directly into an IR detector, its intensity is measured but phase information is lost. Phase information is obtained by allowing the vibrational echo pulse to interfere with another pulse, called the local oscillator. Interference can provide phase information just as in a spatial interference pattern created by two crossed laser beams. In a spatial interference pattern, the fringe pattern is observed as a spatial variation in the intensity, which gives information on the phase relations of the electric fields of the two beams. In the heterodyne-detected vibrational echo experiments, the local oscillator pulse and the vibrational echo pulse are collinear and phase information is obtained by observing the interference pattern (interferogram) as a function of time.

In a dynamic system, the first laser pulse “labels” the initial structures of the species in the sample. The second pulse ends the first time period  $\tau$  and starts clocking the “reaction time”, during which the “labeled” species experience population dynamics. The third pulse ends the population dynamics period of length  $T_w$  and begins a third period of length  $\leq \tau$ , which ends with emission of the echo pulse. The echo signal reads out the information about the final structures of all “labeled” species. There are two types of time periods in the experiment. The periods between the pulses 1 and 2 and between pulse 3 and the echo pulse are called coherence periods. During these periods the vibrations are in coherent superpositions of two vibrational states. Fast vibrational oscillator frequency fluctuations induced by fast structural fluctuation of the system cause dynamic dephasing, which is one contribution to the line shapes in the 2D spectrum. During the period  $T_w$  between pulses 2 and 3, called the population period, a vibration is in a particular state not a superposition state. Slower structural fluctuations of the system, spectral diffusion, contribute to the 2D line shapes. Other processes during the population period also produce changes in the 2D spectrum. For example, chemical exchange can occur in which two species in equilibrium are interconverting one to the other without changing the overall number of either species. Chemical

exchange causes new peaks to grow in as  $T_w$  is increased. In an experiment,  $\tau$  is scanned for fixed  $T_w$ . The recorded signals are converted into a 2D vibrational echo spectrum. Then  $T_w$  is increased and another spectrum is obtained. The series of spectra taken as a function of  $T_w$  provides information on dephasing, spectral diffusion, and population dynamics.

A 2D IR vibrational echo experimental setup is illustrated schematically in Figure 1. Briefly, three successive ultrashort IR pulses with wave vectors (propagation directions)  $k_1$ ,  $k_2$ , and  $k_3$  are applied to the sample to induce the subsequent emission of the time-delayed vibrational echo in a distinct direction ( $k_e = -k_1 + k_2 + k_3$ ). The IR pulses ( $\sim 50$  fs) are produced using a regeneratively amplified Ti:Sapphire laser-pumped optical parametric amplifier system.<sup>31</sup> The vibrational echo pulse is detected with frequency and phase resolution by interfering it with a fifth (local oscillator) pulse, and the combined pulses are dispersed in a monochromator and then detected with a 32-element MCT IR array detector. As discussed above, the function of the local oscillator is to phase resolve (through the interferogram between the echo and local oscillator) and optically heterodyne amplify the vibrational echo signal.

A simple example is given in Figure 2 for the hydroxyl stretch (OD) of phenol-OD in  $\text{CCl}_4$ . Figure 2a shows the linear FT-IR absorption spectrum of the OD stretch. There is a single peak. In the 2D vibrational echo spectrum, there are two frequency axes, which require two Fourier transforms of the time domain data to convert the time structure of the echo into 2D frequency data. As shown in Figure 1, the vibrational echo pulse, which is overlapped with the local oscillator (LO) pulse, is passed through the monochromator. Taking the spectrum of the pulse is an experimental Fourier transform. Thus, one of the two Fourier transforms is performed by the monochromator to provide the vertical axis in the spectrum,  $\omega_m$  (m for monochromator, see Figure 2c). The other axis is obtained by scanning  $\tau$ . Scanning  $\tau$  produces an interferogram (see Figure 2b) as the echo pulse changes its phase relationship relative to the fixed LO pulse. There is one interferogram for each frequency on the  $\omega_m$  axis for which there is signal. The numerical Fourier transforms of these  $\tau$  scan interferograms provide the  $\omega_t$  axis. The data  $S(\omega_t, T_w, \omega_m)$  are then plotted for each  $T_w$  in three dimensions, the amplitude as a function of both  $\omega_t$  and  $\omega_m$ . Details of the method including phase error corrections have been presented.<sup>4,31</sup>

In Figure 2c there is a positive going peak (red) on the diagonal (dashed line) and a negative going peak (blue) off diagonal. The frequency of the first interaction of the radiation field (first pulse) with the vibration is the frequency on the  $\omega_t$  axis. The frequency of the third interaction (third pulse), which is also the frequency of the echo emission, is the frequency on the  $\omega_m$  axis. If  $\omega_m = \omega_t$ , the peak is on the diagonal. This is the situation for the red peak in Figure 2c, which corresponds to the 0–1 vibrational transition of the hydroxyl stretch. In Figure 2c each contour is a 10% change in amplitude. The blue off-

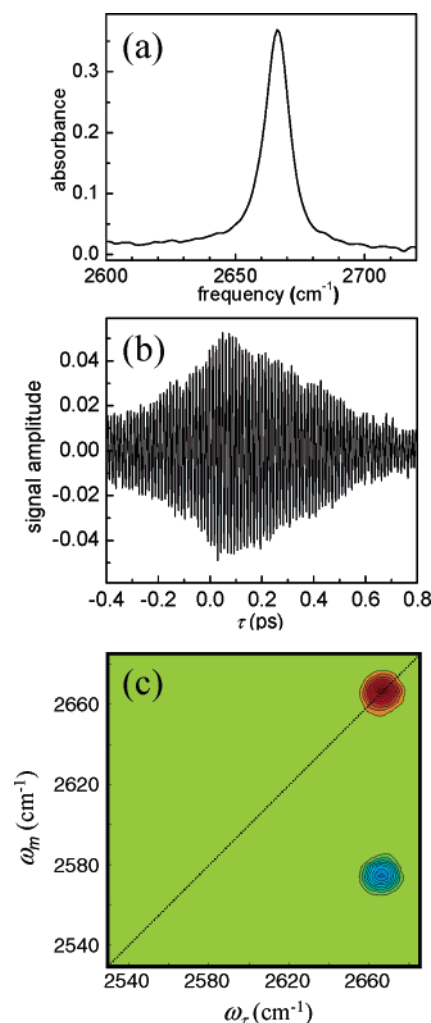


**FIGURE 2.** (a) FTIR spectrum of the hydroxyl stretch (OD) of phenol in  $\text{CCl}_4$ . (b) An interferogram obtained by scanning  $\tau$  for a particular wavelength  $\omega_m$ . (c) 2D IR spectrum of the hydroxyl stretch of phenol in  $\text{CCl}_4$  at  $T_w = 16$  ps.

diagonal peak involves the 1–2 transition. The first interaction produces a coherent superposition state of the 0–1 transition. One of the quantum pathways for the second interaction (second pulse) is to produce a population in the 1 state (first vibrationally excited state). Then the third pulse can couple the 1 state to the 2 state and produce a coherent superposition of 1 and 2. This results in the vibrational echo being emitted at the 1–2 transition frequency, which is shifted to lower frequency than the 0–1 transition by the vibrational anharmonicity. Therefore, the  $\omega_t$  frequency is the 0–1 frequency ( $2670\text{ cm}^{-1}$ ), but the  $\omega_m$  frequency is the 1–2 frequency ( $2570\text{ cm}^{-1}$ ). The off-diagonal anharmonicity peak is negative going because there is a  $180^\circ$  phase shift in the echo pulse electric field relative to the 0–1 echo. The spectrum in Figure 2c is for  $T_w = 16$  ps, a long time compared to the time scale of solvent fluctuations in this system. Therefore, spectral diffusion is complete, and the peaks in the 2D spectrum are symmetrical, essentially round. At short time, the peaks are elongated along the direction of the diagonal. The elongation is the signature of inhomogeneous broadening. As discussed below in connection with

experiments on water, the change in shape with increasing  $T_w$  measures spectral diffusion and, thus, the structural evolution of the system.

### III. Applications

#### A. Solute–Solvent Complexes and Chemical Exchange.

The simplest view of a solute in a liquid solvent is to treat the solvent as a featureless dielectric continuum. A much better description involves the use of a radial distribution function. The radial distribution function describes the probability of finding a solvent molecule some distance from the solute. This model is responsible for the picture of solvent shells surrounding a solute. However, solute and solvent molecules have anisotropic intermolecular interactions that can give rise to well-defined solute–solvent complexes that are not accounted for by a radial distribution function. For organic solute–solvent systems, intermolecular interactions are generally relatively weak, a few kcal/mol. Such weak interactions will produce solute–solvent complexes that are short lived.<sup>9,11,18</sup> Although short lived, the dissociation and formation of organic solute–solvent complexes can influence chemical processes such as reactivity.

Organic solute–solvent complexes are in equilibrium between the complex form and the free solute form. Because formation and dissociation occurs on a picosecond time scale, until recently it has not been possible to observe the chemical exchange process between the two forms of the solute. To discuss the method by which 2D IR vibrational echo spectroscopy can study chemical exchange, it is sufficient to focus on the 0–1 region of the spectrum. Identical considerations apply to the 1–2 region, and analysis of the 1–2 region can provide additional information.<sup>9</sup>

Figure 3 illustrates the influence of chemical exchange on the 2D vibrational echo spectrum. Two species, A and B, with vibrational transition frequencies,  $\omega_A$  and  $\omega_B$ , are in thermal equilibrium. Figure 3a shows the spectrum at short time prior to chemical exchange. There are two peaks on the diagonal: one for species A and one for species B. Figure 3b shows what would happen if A goes to B. The left part of the spectrum is a schematic representation of the combined quantum pathways that lead to the signal.<sup>32</sup> A dashed arrow represents a coherence (coherent superposition state) produced by a radiation field. The solid arrow represents a population, and the curved arrow represents the vibrational echo emission. The first pulse produces coherence between the states of species A at frequency  $\omega_A$ . After time  $\tau$ , the second pulse produces a population. There are several pathways, and a population can be produced in either the ground state (0) or the first excited state (1). During the period  $T_w$  some A's turn into B's ( $A \rightarrow B$ ). The third pulse again produces coherence, but it is coherence of species B at  $\omega_B$  followed by echo emission at  $\omega_B$ . Because the first interaction (frequency on the  $\omega_\tau$  axis) is at  $\omega_A$  but the last interaction and echo emission (frequency on the  $\omega_m$  axis) is at  $\omega_B$ , an

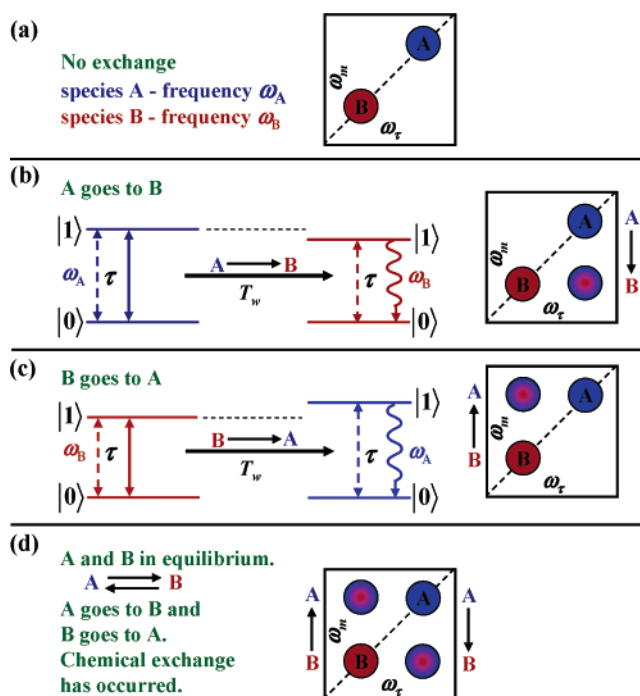
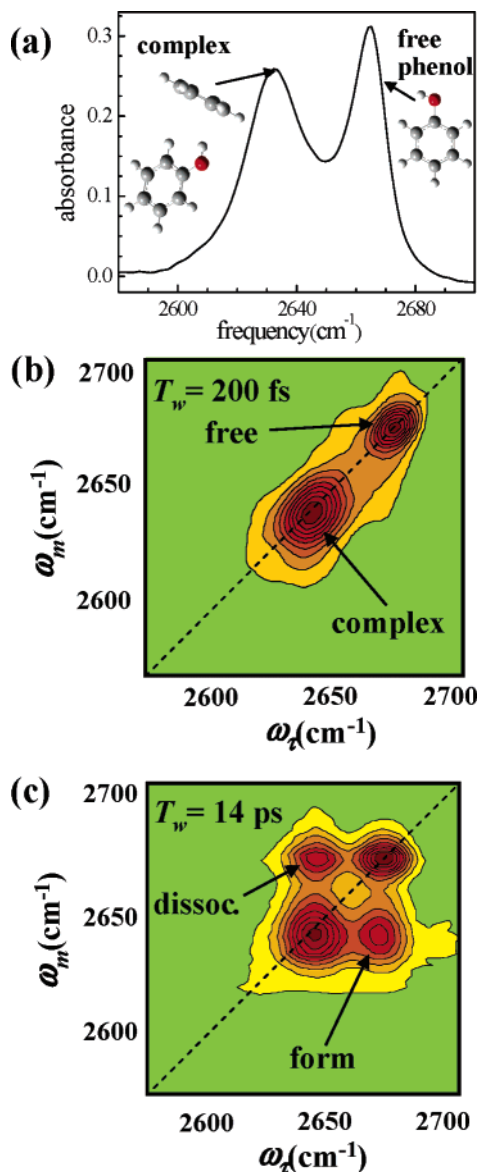


**FIGURE 3.** Schematic illustrations of the observation of chemical exchange between two species A and B. (a) At short time prior to chemical exchange, the two species give two peaks on the diagonal. (b) If some A turns into B, an off-diagonal peak will develop. (c) If some B turns into A, the opposite off-diagonal peak develops. (d) At equilibrium, as much A turns into B as B turns into A, and two equal amplitude off-diagonal peaks are generated.

off-diagonal peak is generated as shown in the right portion of Figure 3b.

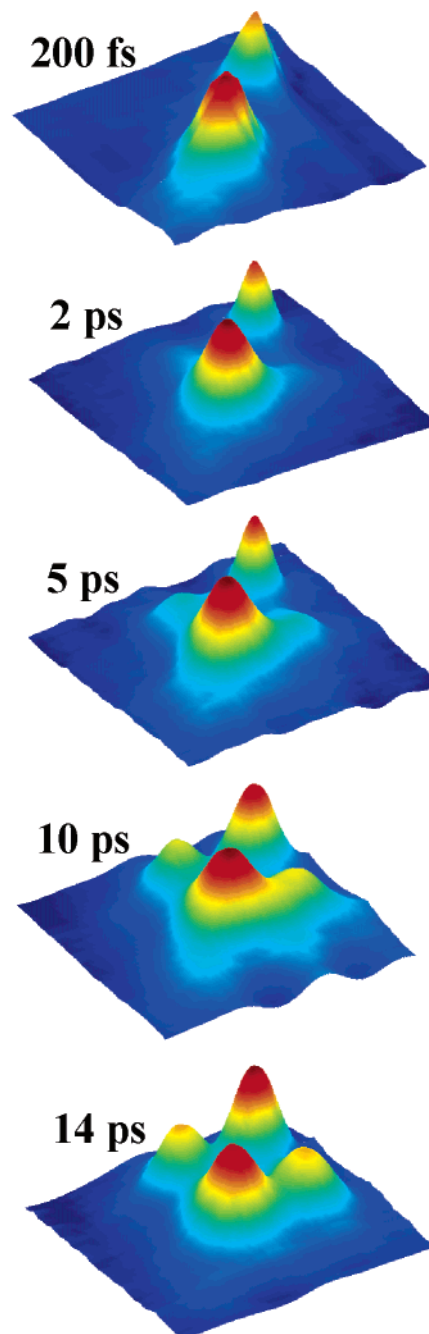
Figure 3c shows what happens if B's turn into A's ( $B \rightarrow A$ ). The first pulse makes a coherence between the 0 and 1 states of B at frequency  $\omega_B$ . The second pulse makes a population on B. If during the period  $T_w$  some B's turn into A's, the third pulse produces a coherence of species A and echo emission from A at frequency  $\omega_A$ . Because the first interaction is at  $\omega_B$  and the last interaction and emission is at  $\omega_A$ , a peak is generated off diagonal as shown in the right portion of Figure 3c. In a real system A and B are in equilibrium. Therefore, the number of A's turning into B's in a given time period is equal to the number of B's turning into A's. As shown in Figure 3d, the result is to produce two off-diagonal peaks. Because some A's and B's may not have undergone chemical exchange or may have undergone chemical exchange but reverted back to the original species prior to the third pulse, there are also diagonal peaks. The model spectrum in Figure 3d is the spectrum for a time long compared to the chemical exchange time, while the spectrum in Figure 3a is for a time short compared to the chemical exchange time. The rate of chemical exchange can be determined by observing the growth of the off-diagonal peaks in the 2D vibrational echo spectrum.<sup>9,11,17,18</sup>

Figure 4a displays the spectrum of the hydroxyl OD stretch of phenol in a mixed solvent of benzene (20 mol %) and  $\text{CCl}_4$  (80 mol %). The high-frequency peak is the free phenol (see Figure 2a). The low-frequency peak is the phenol benzene complex.<sup>9</sup> The structure of the complex,



**FIGURE 4.** (a) FT-IR absorption spectra of the OD stretch of the phenol–benzene complex and free phenol. (b) 2D vibrational echo spectrum prior to significant exchange showing two peaks on the diagonal. (c) 2D spectrum after substantial exchange with two off-diagonal peaks produced by dissociation and formation of the complex.

determined from electronic structure calculations, is shown in the figure.<sup>9</sup> The species are in equilibrium. Complexes are constantly dissociating and free phenols are associating with benzene to form complexes. Figure 4b shows the 2D vibrational echo spectrum at short time,  $T_w = 200$  fs; no significant exchange has occurred. As in Figure 3a, there are two species in the system with different vibrational transition frequencies. At short time, the two species give two peaks on the diagonal, which correspond to the two peaks in the absorption spectrum (Figure 4a). At long time, 14 ps, extensive chemical exchange has occurred. Off-diagonal peaks have grown in as can be seen clearly in Figure 4c. The two peaks correspond to complex dissociation and formation. Figure 4c has the appearance of the schematic shown in Figure 3d, and the discussion surrounding the origin of the off-



**FIGURE 5.** 2D vibrational echo spectra as  $T_w$  increases showing growth of off-diagonal peaks because of chemical exchange.

diagonal peaks in Figure 3 applies to the real data shown in Figure 4.

The growth of the off-diagonal peaks with increasing  $T_w$  can be used to directly determine the thermal equilibrium chemical exchange rate. Figure 5 displays 2D spectra as three-dimensional representations. At 2 ps, the off-diagonal peaks are just appearing in these plots. By 5 ps they are clearly evident and continue to grow as can be seen in the 10 and 14 ps plots. Data like these are used for detailed analysis of the chemical exchange kinetics.<sup>9,11,18</sup> In addition to chemical exchange, there are other dynamical processes that contribute to the time-dependent changes in the spectrum. Spectral diffusion causes the peaks to change shape. The change in shape can be

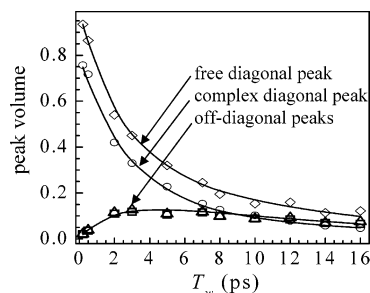


**FIGURE 6.** Peak volumes (symbols) of the four peaks in the 2D spectra vs  $T_w$ . Fits to the data (solid curves) using one adjustable parameter yield the dissociation time, 8 ps.

removed from consideration by fitting the time-dependent peak volumes rather than the peak amplitudes. The vibrational lifetimes of the hydroxyl stretch and the orientational relaxation rates cause all of the peaks to decay in amplitude, while chemical exchange causes the off-diagonal peaks to grow in. The vibrational lifetimes and orientational relaxation rates are measured independently using ultrafast IR pump–probe spectroscopy.<sup>9,11,18</sup> In addition, the equilibrium constant and transition dipole moments of the species are necessary. These are obtained from the FT-IR absorption spectra. With the input constants known, there is only one adjustable parameter to fit the  $T_w$  dependence of all of the peaks in the spectra. Because the rate of complex dissociation is equal to the rate of complex formation, we can fit everything using a *single adjustable parameter*, the complex dissociation time,  $\tau_d = 1/k_{cf}$ , where  $k_{cf}$  is the rate constant for dissociation of the complex (c) to the free form (f).

Figure 6 displays the data and fits for the chemical exchange dynamics of the phenol–benzene complex. There are four peaks in the 2D vibrational echo spectra (see Figures 4 and 5): the two diagonal peaks for the complex and free species and the two off-diagonal peak for  $cf$  and  $f \rightarrow c$ . As can be seen from Figure 6, the data are fit very well with the single parameter  $\tau_d$ . (The mathematical details used to fit the data have been presented.<sup>9,11,18</sup>) The data for the two off-diagonal peaks are identical within experimental error, which is one of the tests that shows that the thermal equilibrium between the complex and free species is not perturbed by the experiments. The results of the fitting yields  $\tau_d = 8$  ps. Experiments in which benzene is replaced by substituted benzenes with electron-withdrawing (bromo) or electron-donating groups (methyls) change the dissociation times because they decrease or increase the  $\pi$  system electron density.<sup>9</sup> Complexes with phenol by bromobenzene, benzene, and *p*-xylene give dissociation times of 6, 8, and 21 ps, respectively. The trend in the dissociation times follows the same trend as the measured enthalpies of formation for the complexes,  $-1.2$ ,  $-1.7$ , and  $-2.2$  kcal/mol, respectively.<sup>9</sup>

In addition to complexes with phenol, other organic solute–solvent complexes have been studied,<sup>18</sup> and more studies are in progress. The 2D vibrational echo chemical exchange method can also be applied to problems such

as isomerization or proton transfer. Experiments to directly examine fast isomerization are in progress.

**B. Water Dynamics.** Water has profound effects on diverse fields of science including chemistry and biology. The properties of liquid water are dominated by the hydrogen bonds among water molecules. The hydrogen bonds produce structured networks that are responsible for water's unique properties. The water hydrogen-bond network is constantly changing over a range of time scales. A water molecule can make zero to four hydrogen bonds that are constantly becoming shorter (stronger) and longer (weaker) and formed and broken. The constantly changing hydrogen-bond networks permit water to accommodate a wide array of chemical processes such as protein folding<sup>33</sup> and ion hydration.<sup>34</sup>

Ultrafast 2D IR vibrational echoes can be used to investigate hydrogen-bond network dynamics in water.<sup>19</sup> When the experimental results are combined with simulations of the experimental observables,<sup>19</sup> a detailed understanding of water emerges. The connection between hydrogen-bond network dynamics and the experiments is through the frequency of the hydroxyl stretch. The frequency of the hydroxyl stretch is lowered (red shifted) when water makes a hydrogen bond.<sup>35</sup> Stronger and more hydrogen bonds cause a greater red shift of the hydroxyl oscillator frequency than weaker and fewer hydrogen bonds.<sup>35,36</sup> As the hydrogen-bond network evolves in time, the strength and number of hydrogen bonds change, which in turn causes the water oscillators' frequencies to change.<sup>19,35,36</sup>

To understand the relationship between the 2D vibrational echo spectrum and the hydrogen-bond dynamics qualitatively an analogy can be made to the chemical exchange experiments discussed in the last section. In the phenol–benzene complex system at short time there are two peaks on the diagonal. At longer times the off-diagonal peaks appear. In water there are a vast number of hydrogen-bonded structures. At short time these structures give rise to an elongated band down the diagonal of the 2D spectrum. As time goes on, exchange of structure makes “off-diagonal” peaks grown in. However, these are not resolved. Instead, on either side of the diagonal effectively continuous groups of off-diagonal peaks grow in. The result is a change in shape of the short time elongated band to a more and more symmetrical band rather than the appearance of new peaks.

To obtain a more quantitative view, consider a single water molecule hydroxyl oscillator. At  $t = 0$ , it will have a particular frequency,  $\omega(0)$ . As the local H-bond structure changes, the frequency will change. At long time, independent of its starting frequency the oscillator can have any frequency in the entire broad hydroxyl stretch absorption spectrum because it has lost memory of its starting frequency (structure). A measure of the frequency evolution, and therefore the structural evolution, is the frequency–frequency correlation function (FFCF). The FFCF is related to the probability that an oscillator with initial frequency  $\omega(0)$  still has the same frequency at time  $t$  later, averaged over all starting frequencies. Vibrational

echo experiments make the FFCF an experimentally observable quantity.<sup>32</sup> The FFCF is the basic input into time-dependent diagrammatic perturbation theory that is used to calculate nonlinear optical experimental observables in general<sup>32</sup> and vibrational echo signals in particular.<sup>19</sup> The FFCF and diagrammatic perturbation theory should provide an accurate description for systems such as phenol complexes. However, for water recent theoretical work has shown that it is necessary to go beyond diagrammatic perturbation theory because of non-Condon effects that influence experimental observables.<sup>37</sup> Nonetheless, even for water the FFCF provides important qualitative insights and an almost quantitative description of water dynamics.

The experiments<sup>19</sup> and simulations<sup>19,38</sup> look at the time evolution of the hydroxyl stretching frequency (the OD stretch of low concentration HOD in H<sub>2</sub>O), which reports on the structural evolution of the water network. HOD is used to avoid vibrational excitation transfer, which would influence the experiments and is not a ground-state equilibrium process. Figure 7 displays 2D vibrational echo spectra of water as a function of  $T_w$ . The figure shows both the 0–1 (red, positive going) and 1–2 (blue, negative going) OD hydroxyl stretch transitions. Each contour represents a 10% change in signal. At 100 fs (top) the 0–1 band is substantially elongated along the diagonal. As time increases, the band changes shape and becomes increasingly symmetrical. By 1.6 ps, the 0–1 band is basically symmetrical along the  $\omega$  axis. It would be essentially round, but the overlap with the negative going 1–2 band eats away the bottom portion.

The change in shape is directly related to the structural evolution of the hydrogen-bond network. When the shape becomes symmetrical, all hydrogen-bond structural configurations have been sampled, which happens by  $\sim 3$  ps. Data such as those presented in Figure 7 can be analyzed quantitatively to extract the FFCF. The experimental FFCF is compared to FFCFs obtained from simulations of water to determine the nature of the hydrogen-bond network motions on different time scales.<sup>19,38,39</sup> The results show that the shortest time scale fluctuations (less than a few hundred femtoseconds) involve very local hydrogen-bond motions mainly of the length of a hydrogen bond. The longer time scale dynamics are global hydrogen-bond network rearrangements that lead to complete randomization of the water structure. The 2D vibrational echo results determined this slowest component of the FFCF to be 1.5 ps. This is the time scale on which the water hydrogen-bond network restructures to accommodate processes such as solvation or protein folding.

**C. Chemical Structure Analysis.** 2D vibrational echoes can also find uses in chemical analysis.<sup>15</sup> Frequently a molecule will have several modes of the same type on a single molecule, for example, the various C–H stretching modes of toluene. In a mixture of two or more unknown chemical species, it can be difficult to determine which peaks in an IR spectrum belong to a particular molecule or even how many molecules are in the mixture by examining the linear IR spectrum.

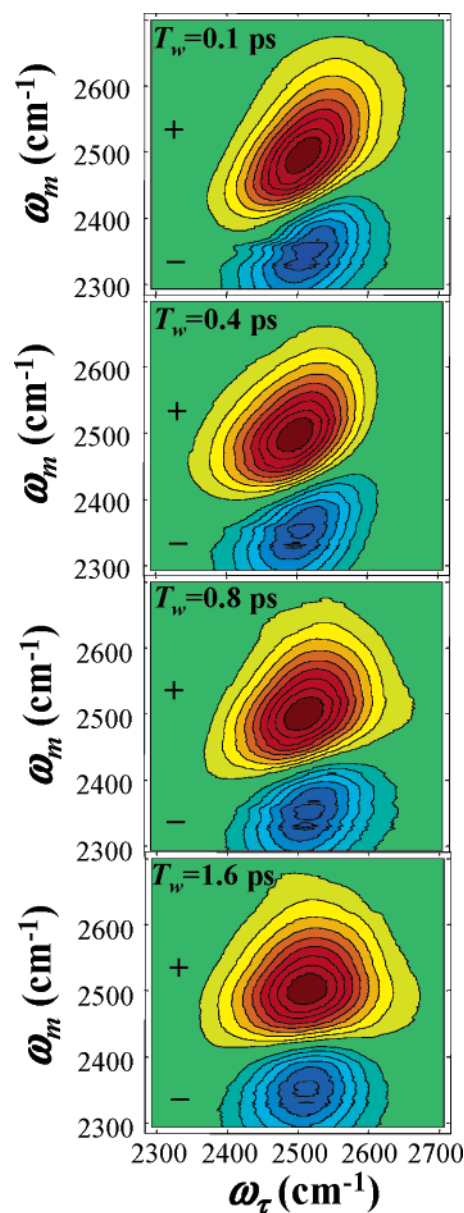


**FIGURE 7.** 2D vibrational echo spectra of the OD stretch of HOD in water as a function of  $T_w$  showing the 0–1 transition (red) and the 1–2 transition (blue). The change in shape of the bands with  $T_w$  yields the hydrogen-bond network dynamics.

Vibrational modes on a molecule can be coupled through anharmonic terms in the vibrational potential. In 2D NMR magnetic dipole–magnetic dipole coupling between spins produces off-diagonal peaks. In the 2D IR spectrum coupling between vibrational modes of a molecule also produces off-diagonal peaks. In a mixture of molecules, the off-diagonal peaks can be useful in determining which peaks in an FT-IR absorption spectrum belong to the same molecule.<sup>15</sup>

Figure 8a shows an absorption spectrum with four peaks in the IR region that corresponds to metal carbonyl CO stretching modes. From the absorption spectrum it is not possible to determine if there are four molecules each with one mode, one molecule with four modes, or anything in between. In a 2D IR vibrational echo spectrum there are peaks that only correspond to transitions involv-

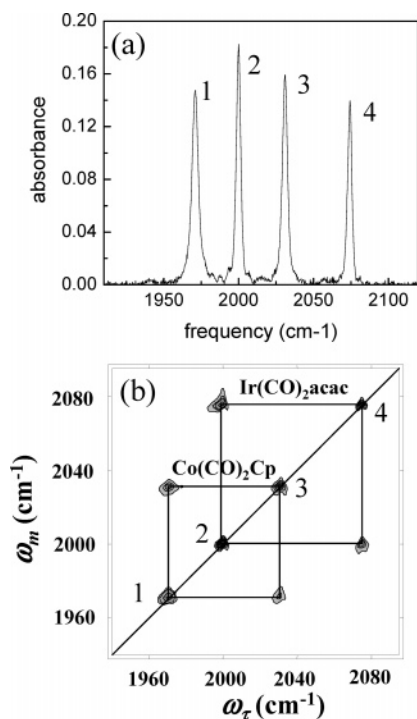


**FIGURE 8.** (a) FT-IR spectrum of the carbonyl stretch region for a mixed solution of  $\text{Ir}(\text{CO})_2(\text{acac})$  and  $\text{Co}(\text{CO})_2\text{Cp}$  in hexane. (b) 2D IR vibrational echo spectrum of the same sample showing the positive peaks only. The off-diagonal peaks show which diagonal peaks are coupled by anharmonic terms in the molecular potential and, therefore, which peaks belong to the same molecule. The lines are aids to the eye.

ing 0 and 1 states and peaks that require the 1 state to first be populated. These two types of peaks are easily distinguishable by their sign (see Figure 2c and 7).<sup>4,15</sup>

Figure 8b shows a 2D vibrational echo spectrum of the same sample that gave the spectrum in Figure 8a.<sup>15</sup> Only the eight positive peaks are shown. The sample is a mixture of two metal dicarbonyls, (acetylacetonato)dicarbonyliridium ( $\text{Ir}(\text{CO})_2(\text{acac})$ ) and (cyclopentadienyl)dicarbonylcobalt ( $\text{Co}(\text{CO})_2\text{Cp}$ ) in hexane. Each metal carbonyl has two modes that give rise to two peaks in the absorption spectrum. The result is four peaks in the absorption spectrum and four peaks on the diagonal of the 2D spectrum. However, in addition to the diagonal peaks in the 2D spectrum, there are off-diagonal peaks. Modes that are on the same molecule and coupled via anharmonic terms in the potential generate “coherence transfer” peaks, which form a square with the diagonal peaks that are coupled<sup>4</sup> and therefore on the same molecule.<sup>15</sup> It is clear from the 2D spectrum that there are pairs of coupled peaks. The four peaks in Figure 8a are composed of two pairs of peaks, with peaks 1 and 3 going together and peaks 2 and 4 going together. The peaks corresponding to the two molecules are labeled in Figure 8b. Thus, additional information on mixtures of molecules can be obtained from the 2D spectrum. Because the 2D vibrational echo measurements occur on an ultrafast time scale, it is possible to perform such experiments in reaction mixtures to help identify short-lived intermediates and products.

## IV. Concluding Remarks

Ultrafast infrared 2D vibrational echo spectroscopy is an emerging tool for the study of chemical, biological, and materials problems. In the early days of NMR home-built machines were used to do the initial experiments. Now ultrasophisticated multidimensional NMR instruments can be purchased as commercial packages. The laser equipment necessary to perform the ultrafast IR experiments is improving rapidly. The very complex optics, electronics, and computer software necessary to perform the 2D IR experiments are also advancing rapidly. It is easy to envision a future in which ultrafast multidimensional IR vibrational echo spectroscopy and related experiments will be as accessible to the scientific community as NMR.

*The authors gratefully acknowledge John B. Asbury, Tobias Steinel, Christopher Stromberg, and Xin Chen, who were involved in many of the experiments that are discussed in this paper. This research was supported by a grant from the AFOSR (F49620-01-1-0018) and NSF (DMR-0332692).*

## References

- (1) Zimdars, D.; Tokmakoff, A.; Chen, S.; Greenfield, S. R.; Fayer, M. D.; Smith, T. I.; Schwetman, H. A. Picosecond Infrared Vibrational Echoes in a Liquid and Glass Using a Free Electron Laser. *Phys. Rev. Lett.* **1993**, *70*, 2718–2721.
- (2) Merchant, K. A.; Thompson, D. E.; Fayer, M. D. Two-Dimensional Time-Frequency Ultrafast Infrared Vibrational Echo Spectroscopy. *Phys. Rev. Lett.* **2001**, *86*, 3899–3902.
- (3) Zanni, M. T.; Hochstrasser, R. M. Two-Dimensional Infrared Spectroscopy: A Promising New Method for the Time Resolution of Structures. *Curr. Opin. Struct. Biol.* **2001**, *11*, 516–522.
- (4) Khalil, M.; Demirdoven, N.; Tokmakoff, A. Obtaining Absorptive Line Shapes in Two-Dimensional Infrared Vibrational Correlation Spectra. *Phys. Rev. Lett.* **2003**, *90*, 047401(4).
- (5) Khalil, M.; Demirdoven, N.; Tokmakoff, A. Vibrational Coherence Transfer Characterized with Fourier-Transform 2D IR Spectroscopy. *J. Chem. Phys.* **2004**, *121*, 362–373.
- (6) Asbury, J. B.; Steinel, T.; Fayer, M. D. Hydrogen Bond Networks: Structure and Evolution after Hydrogen Bond Breaking. *J. Phys. Chem. B* **2004**, *108*, 6544–6554.
- (7) Mukherjee, P.; Krummel, A. T.; Fulmer, E. C.; Kass, I.; Arkin, I. T.; Zanni, M. T. Site-Specific Vibrational Dynamics of the Cd3 Zeta Membrane Peptide Using Heterodyned Two-Dimensional Infrared Photon Echo Spectroscopy. *J. Chem. Phys.* **2004**, *120*, 10215–10224.
- (8) Fulmer, E. C.; Ding, F.; Zanni, M. T. Heterodyned Fifth-Order 2D-IR Spectroscopy of the Azide Ion in an Ionic Glass. *J. Chem. Phys.* **2005**, *122*, 034302(12).
- (9) Zheng, J.; Kwak, K.; Asbury, J. B.; Chen, X.; Piletic, I.; Fayer, M. D. Ultrafast Dynamics of Solute-Solvent Complexation Observed at Thermal Equilibrium in Real Time. *Science* **2005**, *309*, 1338–1343.
- (10) DeCamp, M. F.; DeFlores, L.; McCracken, J. M.; Tokmakoff, A.; Kwak, K.; Cho, M. Amide I Vibrational Dynamics of *N*-Methylacetamide in Polar Solvents: The Role of Electrostatic Interactions. *J. Phys. Chem. B* **2005**, *109*, 11016–11026.
- (11) Kwak, K.; Zheng, J.; Cang, H.; Fayer, M. D. Ultrafast 2D IR Vibrational Echo Chemical Exchange Experiments and Theory. *J. Phys. Chem. B* **2006**, accepted for publication.
- (12) Scheurer, C.; Mukamel, S. Magnetic Resonance Analogies in Multidimensional Vibrational Spectroscopy. *Bull. Chem. Soc. Jpn.* **2002**, *75*, 989–999.
- (13) Mukamel, S. Multidimensional Femtosecond Correlation Spectroscopies of Electronic and Vibrational Excitations. *Ann. Rev. Phys. Chem.* **2000**, *51*, 691–729.
- (14) Golonzka, O.; Tokmakoff, A. Polarization-Selective Third-Order Spectroscopy of Coupled Vibronic States. *J. Chem. Phys.* **2001**, *115*, 297–309.
- (15) Asbury, J. B.; Steinel, T.; Fayer, M. D. Using Ultrafast Infrared Multidimensional Correlation Spectroscopy to Aid in Vibrational Spectral Peak Assignments. *Chem. Phys. Lett.* **2003**, *381*, 139–146.

- (16) Merchant, K. A.; Noid, W. G.; Akiyama, R.; Finkelstein, I.; Goun, A.; McClain, B. L.; Loring, R. F.; Fayer, M. D. Myoglobin-CO Substate Structures and Dynamics: Multidimensional Vibrational Echoes and Molecular Dynamics Simulations. *J. Am. Chem. Soc.* **2003**, *125*, 13804–13818.
- (17) Kim, Y. S.; Hochstrasser, R. M. Chemical Exchange 2D IR of Hydrogen-Bond Making and Breaking. *Proc. Natl. Acad. Sci.* **2005**, *102*, 11185–11190.
- (18) Zheng, J.; Kwak, K.; Chen, X.; Asbury, J. B.; Fayer, M. D. Formation and Dissociation of Intra-Intermolecular Hydrogen Bonded Solute-Solvent Complexes: Chemical Exchange 2D IR Vibrational Echo Spectroscopy. *J. Am. Chem. Soc.* **2006**, *128*, 2977–2987.
- (19) Asbury, J. B.; Steinel, T.; Kwak, K.; Corcelli, S.; Lawrence, C. P.; Skinner, J. L.; Fayer, M. D. Dynamics of Water Probed with Vibrational Echo Correlation Spectroscopy. *J. Chem. Phys.* **2004**, *121*, 12431–12446.
- (20) Fecko, C. J.; Eaves, J. D.; Loparo, J. J.; Tokmakoff, A.; Geissler, P. L. Local and Collective Hydrogen Bond Dynamics in the Ultrafast Vibrational Spectroscopy of Liquid Water. *Science* **2003**, *301*, 1698–1702.
- (21) Merchant, K. A.; Noid, W. G.; Thompson, D. E.; Akiyama, R.; Loring, R. F.; Fayer, M. D. Structural Assignments and Dynamics of the  $\alpha$  Substates of Mbco: Spectrally Resolved Vibrational Echo Experiments and Molecular Dynamics Simulations. *J. Phys. Chem. B* **2003**, *107*, 4–7.
- (22) Tokmakoff, A.; Fayer, M. D. Infrared Photon Echo Experiments: Exploring Vibrational Dynamics in Liquids and Glasses. *Acc. Chem. Res.* **1995**, *28*, 437–445.
- (23) Tokmakoff, A.; Zimdars, D.; Sauter, B.; Francis, R. S.; Kwok, A. S.; Fayer, M. D. Vibrational Photon Echoes in a Liquid and Glass: Room Temperature to 10 K. *J. Chem. Phys.* **1994**, *101*, 1741.
- (24) Tokmakoff, A.; Kwok, A. S.; Urdahl, R. S.; Francis, R. S.; Fayer, M. D. Multilevel Vibrational Dephasing and Vibrational Anharmonicity from Infrared Photon Echo Beats. *Chem. Phys. Lett.* **1995**, *234*, 289.
- (25) Asplund, M. C.; Lim, M.; Hochstrasser, R. M. Spectrally Resolved Three Pulse Photon Echoes in the Vibrational Infrared. *Chem. Phys. Lett.* **2000**, *323*, 269–277.
- (26) Kim, Y.; Hochstrasser, R. M. Dynamics of Amide-I Modes of the Alanine Dipeptide in D<sub>2</sub>O. *J. Phys. Chem. B* **2005**, *109*, 6884–6891.
- (27) Piletic, I.; Moilanen, D. E.; Spry, D. B.; Levinger, N. E.; Fayer, M. D. Testing the Core/Shell Model of Nanoconfined Water in Reverse Micelles Using Linear and Nonlinear IR Spectroscopy. *J. Phys. Chem. A* **2006**, *110*, 4985–4999.
- (28) Massari, A. M.; Finkelstein, I. J.; Fayer, M. D. Dynamics of Proteins Encapsulated in Silica Sol-Gel Glasses Studied with IR Vibrational Echo Spectroscopy. *J. Am. Chem. Soc.* **2006**, *128*, 3990–3997.
- (29) Hahn, E. L. Spin Echoes. *Phys. Rev.* **1950**, *80*, 580–594.
- (30) Abella, I. D.; Kurnit, N. A.; Hartmann, S. R. Photon Echoes. *Phys. Rev.* **1966**, *14*, 391–406.
- (31) Asbury, J. B.; Steinel, T.; Fayer, M. D. Vibrational Echo Correlation Spectroscopy Probes Hydrogen Bond Dynamics in Water and Methanol. *J. Lumin.* **2004**, *107*, 271–286.
- (32) Mukamel, S. *Principles of Nonlinear Optical Spectroscopy*; Oxford University Press: New York, 1995.
- (33) Daggett, V.; Fersht, A. The Present View of the Mechanism of Protein Folding. *Nat. Rev. Mol. Cell Biol.* **2003**, *4*, 497–502.
- (34) Spangberg, D.; Rey, R.; Hynes, J. T.; Hermansson, K. Rate and Mechanisms for Water Exchange around Li<sup>+</sup>(Aq) from Md Simulations. *J. Phys. Chem. B* **2003**, *107*, 4470–4477.
- (35) Lawrence, C. P.; Skinner, J. L. Vibrational Spectroscopy of HOD in Liquid D<sub>2</sub>O. III. Spectral Diffusion, and Hydrogen-Bonding and Rotational Dynamics. *J. Chem. Phys.* **2003**, *118*, 264–272.
- (36) Lawrence, C. P.; Skinner, J. L. Vibrational Spectroscopy of HOD in Liquid D<sub>2</sub>O. I. Vibrational Energy Relaxation. *J. Chem. Phys.* **2002**, *117*, 5827.
- (37) Schmidt, J. R.; Corcelli, S. A.; Skinner, J. L. Pronounced Non-Condon Effects in the Ultrafast Infrared Spectroscopy of Water. *J. Chem. Phys.* **2005**, *123*, 044513(13).
- (38) Corcelli, S.; Lawrence, C. P.; Skinner, J. L. Combined Electronic Structure/Molecular Dynamics Approach for Ultrafast Infrared Spectroscopy of Dilute HOD in Liquid H<sub>2</sub>O and D<sub>2</sub>O. *J. Chem. Phys.* **2004**, *120*, 8107.
- (39) Møller, K. B.; Rey, R.; Hynes, J. T. Hydrogen Bond Dynamics in Water and Ultrafast Infrared Spectroscopy: A Theoretical Study. *J. Phys. Chem. A* **2004**, *108*, 1275–1289.

AR068010D